Local approach to electronic excitations in MnO, FeO, CoO, and NiO

Manabu Takahashi and Jun-ichi Igarashi
Faculty of Engineering, Gunma University, Kiryu, Gunma 376, Japan
(Received 6 June 1996; revised manuscript received 26 July 1996)

The excitation spectra of the antiferromagnetic transition-metal oxides MnO, FeO, CoO, and NiO are studied by developing a local three-body scattering theory within a multiorbital tight-binding model. The self-energy corrections to the Hartree-Fock solutions are carried out by taking account of local three-body correlations. Thereby the multiplet structures of three-particle states are fully taken into account. It is shown that the self-energy correction improves drastically the excitation spectra for FeO, CoO, and NiO, leading to the correct value of the band gap and the satellite structure, in agreement with photoemission experiments. Quasiparticle dispersions are obtained in good agreement with the angle-resolved photoemission data of CoO and NiO. The self-energy correction for MnO is found to be quite small. [S0163-1829(96)07043-9]

I. INTRODUCTION

Much attention was paid in the past to the electronic structure of narrow-band transition-metal compounds. They exhibit a variety of electronic and magnetic properties. For example, the ground state can be insulating, semiconducting, metallic, superconducting, ferromagnetic, ferrimagnetic, or antiferromagnetic. Electron correlations due to their mutual Coulomb repulsions are considered to play an important role.[1] In this paper, we concentrate our attention on the late transition-metal monoxides MnO, FeO, CoO, and NiO. They are antiferromagnetic insulators of the second kind with a rocksalt structure, and can be considered prototypes of materials with strong electron correlations.

Electronic band-structure calculations for solids are based in most cases on the local-density approximation (LDA) to density functional theory. Calculations of this kind often give results in agreement with corresponding x-ray photoemission (XPS) experiments and bremsstrahlung isochromat spectroscopy (BIS). However, when the LDA is applied to strongly correlated electron systems such as high-T_c cuprates or transition-metal compounds, it shows a number of weaknesses. For transition-metal oxides it underestimates the size of band gap by an order of magnitude. It may even predict metallic behavior for large gap materials.[2] Magnetic moments usually came out too small as compared with experiments.[3–8] The satellite intensity below the valence band observed clearly in XPS experiments on CoO and NiO is not reproduced.[9] It is puzzling, that in spite of these shortcomings, the LDA bands seem to fit well the energy dispersions determined from angle-resolved photoemission spectroscopy (ARPS).[10–12]

Another approach which has been applied is the cluster or impurity model method,[13–16] in which transition-metal ions are treated like impurities in an O $2p$ host. By fitting the free parameters of that model, it is able to explain the experimental data of XPS,[9,13,15,17–24] BIS,[18,21–23] resonant photoemission,[16,20,25–27] and core-level photoabsorption.[14,22,23] For NiO and CoO these analyses suggest that the gap is of charge-transfer type,[13,28] instead of the conventional Mott-Hubbard type,[1,29] that is, the $3d$ bands are split into upper and lower Hubbard bands separated by a Coulomb energy U, with the oxygen band placed between them. Accordingly in NiO and CoO the first ionized state is found to have a strong O $2p$ character.[13,21–23,30] This differs from LDA findings in that the top of the valence band is predominantly of Ni $3d$ character, and that the O $2p$ bands are located well below the Ni $3d$ bands. A major difficulty of the cluster models is that they are unable to describe the energy bands which recently were determined by ARPS experiments.[10–12,31–33]

Several attempts have been undertaken to improve the LDA. We especially mention the LDA$+U$ method[34] and a self-interaction correction to the LDA.[35–37] When applied to transition-metal oxides, both theories correctly predict an insulating ground state. They tend to overestimate the charge transfer, however, and do not reproduce the observed photoemission results. Another popular approach is based on a GW approximation, and accounts for electron correlations in the frame of the LDA scheme.[38] For NiO,[39] the quasiparticle energies are considerably improved compared with those of the LDA, but the satellite structure is not reproduced. This shortcoming is ascribed to the fact that the GW approximation takes account of bubble-type diagrams but not of ladder-type diagrams, giving rise to satellite intensities. Since the LDA already contains correlations to some extent, it is difficult to see how one can improve a correlation treatment in a controlled fashion by starting from that scheme. It seems preferable to start from a Hartree-Fock (HF) approximation and then to include the effects of electron correlations. This is the approach we want to pursue here. Although *ab initio* HF calculations for solids have become feasible,[40] the inclusion of self-energy effects on an *ab initio* level is presently not yet possible. Therefore one has to resort to a multiorbital tight-binding model with parameters determined either from a cluster or impurity model analysis of experiments. The results obtained within the HF approximation resemble those of the LDA$+U$ and SIC methods.

The self-energy contributions are evaluated on the basis of the three-body scattering theory proposed by one of the present authors.[41,42] This theory was originally developed in order to study the effects of electron correlations on ferromagnetic Ni. From the theory of Kanamori,[43] the effects of multiple hole-hole scattering are known. Although that theory seems particularly valid in the limit of low hole densities, it proved insufficient in order to account for the ob-

served photoemission spectra of ferromagnetic Ni metal.[44] To improve the situation, theories were proposed which also take into account multiple electron-hole scattering.[45,46] The three-body scattering theory proposed by one of the authors[41,42] is based on Faddeev's equation,[47] and treats simultaneously multiple electron-electron, hole-hole, and electron-hole scattering processes. This theory considerably improved the results of the low-density approximation, and successfully described the excitation spectra by using a simple Hubbard-type model. This success suggests that the creation of many electron-hole pairs neglected in that theory is of minor importance except for small excitation energies.

Solving the Faddeev equation is quite difficult for a multiorbital tight-binding model which has to be used for a quantitative comparison with experiments. Therefore we make a local approximation which limits the three-body scattering processes to different transition-metal sites. This approximation is expected to cover the most important correlation effects, but a future improved theory should also take into account the local correlations on the O sites. It has been shown that the local approximation works well for ferromagnetic Ni, and yields an excitation spectrum in good agreement with photoemission experiments.[48] Here we extend the formulation to unit cells with several atoms and nonvanishing off-diagonal matrix elements of the Coulomb part of the Fock matrix. A short account of the application of this theory to antiferromagnetic NiO has already been reported.[49] We shall demonstrate that the self-energy calculated in this way for transition-metal oxides results in a transfer of spectral weight, a shift of the $3d$ levels, and the appearance of satellite structures. The excitation spectra of NiO, CoO, and FeO are thereby drastically improved, and are found to be in good agreement with the XPS, BIS, and O $K\alpha$ x-ray emission spectroscopy (XES) experiments.[50] For MnO the self-energy contribution is found to be small. This is related to the half-filled $3d$ shell of Mn. It should be noted that the theory considered here contains bubble-type diagrams, despite the restriction to on-site scattering processes.

In Sec. II we formulate a local three-body scattering theory for the multiorbital tight-binding model. In Sec. III, the theory is applied to antiferromagnetic MnO, FeO, and CoO, and NiO. The results are compared with the experiments of XPS, BIS, O $K\alpha$ XES, and ARPS. Section IV contains concluding remarks.

TABLE I. Parameter values for the tight-binding model of MnO, FeO, CoO, and NiO in units of eV.

Parameter	MnO	FeO	CoO	NiO
A	3.9	5.5	5.2	5.6
B	0.12	0.13	0.14	0.13
C	0.41	0.48	0.54	0.60
Δ	8.8	7.0	5.5	5.0
$pd\sigma$	1.3	1.3	1.3	1.4
$pd\pi$	−0.6	−0.6	−0.6	−0.63
$pp\sigma$	0.55	0.55	0.55	0.60
$pp\pi$	−0.15	−0.15	−0.15	−0.15
$dd\sigma$	−0.23	−0.29	−0.25	−0.23
$dd\pi$	0.025	0.030	0.058	0.10
$dd\delta$	−0.005	−0.004	−0.006	−0.01
$10Dq$	0.70	0.70	0.70	0.70

II. FORMULATION

We employ a multiorbital tight-binding model defined by

$$H=H_0+H_I, \tag{2.1}$$

$$\begin{aligned} H_0=&\sum_{im\sigma} E^d(m)n^d_{im\sigma}+\sum_{jl\sigma} E^p n^p_{jl\sigma} \\ &+\sum_{\langle i,j\rangle}\sum_{\sigma lm}(t^{dp}_{im,jl}d^\dagger_{im\sigma}p_{jl\sigma}+\text{H.c.}) \\ &+\sum_{\langle j,j'\rangle}\sum_{\sigma ll'}(t^{pp}_{jl,j'l'}p^\dagger_{jl\sigma}p_{j'l'\sigma}+\text{H.c.}) \\ &+\sum_{\langle i,i'\rangle}\sum_{\sigma mm'}(t^{dd}_{im,i'm'}d^\dagger_{im\sigma}d_{i'm'\sigma}+\text{H.c.}), \end{aligned} \tag{2.2}$$

$$H_I=\tfrac{1}{2}\sum_i \sum_{\nu_1\nu_2\nu_3\nu_4} g(\nu_1\nu_2\nu_3\nu_4)d^\dagger_{i\nu_1}d^\dagger_{i\nu_2}d_{i\nu_4}d_{i\nu_3}. \tag{2.3}$$

H_0 represents the kinetic energy. Operators $d_{im\sigma}$ and $p_{jl\sigma}$ denote the annihilation of an electron with spin σ in the $3d$ orbit m of the transition-metal (TM) site i and the annihilation of an electron with spin σ in the $2p$ orbit l of the O site j, respectively. Number operators $n^d_{im\sigma}$ and $n^p_{jl\sigma}$ are defined by $n^d_{im\sigma}=d^\dagger_{im\sigma}d_{im\sigma}$, and $n^p_{jl\sigma}=p^\dagger_{jl\sigma}p_{jl\sigma}$. The transfer integrals $t^{dp}_{im,jl}$, $t^{pp}_{jl,j'l'}$, and $t^{dd}_{im,i'm'}$ are evaluated from the Slater-Koster two-center integrals $(pd\sigma)$, $(pd\pi)$, $(pp\sigma)$, $(pp\pi)$, $(dd\sigma)$, $(dd\pi)$, and $(dd\delta)$.[51] A point charge crystal-field splitting $(10Dq)$ is taken into account so that the $3d$ orbital energies are split according to $E^d(e_g)=E^d+6Dq$, and $E^d(t_{2g})=E^d-4Dq$. The d-level position relative to the p levels is given by the charge-transfer energy Δ defined by $\Delta=E_d-E_p+nU$ for the d^n configuration. Here U is the multiplet-averaged d-d Coulomb interaction given by $U=A-14B/9+7C/9$. H_I represents the intra-atomic Coulomb interaction on TM sites. The Coulomb interaction on O sites is neglected. The interaction matrix element $g(\nu_1\nu_2\nu_3\nu_4)$ is written in terms of the Racah parameters A, B, and C, where the abbreviation ν stands for (m,σ).

We determine most parameter values from a cluster-model analysis of photoemission spectra.[21–23] The values for $(dd\sigma)$, $(dd\pi)$, and $(dd\delta)$ cannot be determined from the cluster-model analysis, and therefore we set them close to Mattheiss' LDA estimates.[52] Among the Racah parameters, B and C are known to be little screened by solid-state effects, while A is known to be considerably screened. For B and C we use the atomic values, but regard the value of A as an adjustable parameter so as to obtain a reasonable satellite position. As a result, we find a value of A which is roughly 1 eV smaller than that obtained from the cluster-model analysis.[23] Table I lists the parameter values used in the present calculation.

For MnO, FeO, CoO, and NiO we assume an antiferromagnetic structure of the second kind, and divide the TM sites into two sublattices A and B. In Ref. 49, for NiO, we described the procedures to make the HF approximation and

to calculate the self-energy. In the following we mention mainly the altered points to deal with the complicated situation of FeO and CoO.

In the HF approximation for NiO, we defined the $3d$ orbits by $m=xy$, yz, zx, x^2-y^2, and $3z^2-r^2$, with x, y, and z referring to the crystal axes. In this case only the diagonal parts of $\langle g|d^\dagger_{i\nu}d_{i\nu'}|g\rangle$ (with $|g\rangle$ denoting the HF ground state) remain as nonvanishing elements. For FeO and CoO, however, the off-diagonal parts do not vanish, complicating the self-consistent determination of the HF potential. This requires matrix forms of the on-site HF energies for the later calculation of the self-energy:

$$\epsilon_{i\nu,i\nu'}=\sum_{n,\mathbf{k}\notin\tilde{F}}(e_{n,\mathbf{k}}-\mu_0)f^*_{n,\mathbf{k}}(i\nu)f_{n,\mathbf{k}}(i\nu'), \tag{2.4}$$

$$\overline{\epsilon}_{i\nu,i\nu'}=\sum_{n,\mathbf{k}\in\tilde{F}}(e_{n,\mathbf{k}}-\mu_0)f^*_{n,\mathbf{k}}(i\nu)f_{n,\mathbf{k}}(i\nu'). \tag{2.5}$$

Here the HF eigenvalues are classified according to momentum $\mathbf{k}$ and band label n, and are denoted as $e_{n,\mathbf{k}}$. The corresponding wave functions are $f_{n,\mathbf{k}}(im\sigma)$ and $f_{n,\mathbf{k}}(jl\sigma)$. Symbol $\tilde{F}$ represents the Fermi volume, i.e., the volume occupied by electrons in momentum space, and μ_0 is the HF chemical potential. In addition, the density matrix $n_{i\nu,i\nu'}$ for electrons and $\overline{n}_{i\nu,i\nu'}$ for holes are also necessary for the later calculation of the self-energy. They are defined as

$$n_{i\nu,i\nu'}=\sum_{n,\mathbf{k}\notin\tilde{F}}f^*_{n,\mathbf{k}}(i\nu)f_{n,\mathbf{k}}(i\nu'), \tag{2.6}$$

$$\overline{n}_{i\nu,i\nu'}=\sum_{n,\mathbf{k}\in\tilde{F}}f^*_{n,\mathbf{k}}(i\nu)f_{n,\mathbf{k}}(i\nu'). \tag{2.7}$$

The mean energies of an electron and a hole in orbit ν at site i defined as $e_{i\nu}$ and $\overline{e_{i\nu}}$ in Ref. 49 are now given by $e_{i\nu}=\epsilon_{i\nu,i\nu}/n_{i\nu,i\nu}$ and $\overline{e}_{i\nu}=\overline{\epsilon}_{i\nu,i\nu}/\overline{n}_{i\nu,i\nu}$.

The single-particle Green's functions are introduced in the same form as before,

$$G^{dd}_{m\sigma,m'\sigma'}(i,i';t)=-i\langle T(d_{im\sigma}(t)d^\dagger_{i'm'\sigma'}(0))\rangle, \tag{2.8}$$

$$G^{pp}_{l\sigma,l'\sigma'}(j,j';t)=-i\langle T(p_{jl\sigma}(t)p^\dagger_{j'l'\sigma'}(0))\rangle, \tag{2.9}$$

where T is the time ordering operator, $\langle\ \rangle$ denotes the average over the ground state, and $d_{im\sigma}(t)=\exp[i(H-\mu N_e)t]d_{im\sigma}\exp[-i(H-\mu N_e)t]$, with μ and N_e denoting the chemical potential and the number operator of electrons. We take $H_0+H_I^{\mathrm{HF}}$ as the unperturbed Hamiltonian, and calculate only the diagonal part of the self-energy with respect to TM sites. This gives the main contribution to the self-energy, since the Coulomb interaction acts only on TM sites. For calculating the self-energy, we need to introduce the three-particle states $|R;i,\nu_1,\nu_2,\nu_3\rangle$,$|A;i,\nu_1,\nu_2,\nu_3\rangle$, which are defined by Eqs. (2.12) and (2.13) in Ref. 49. Although they are orthogonal to each other for NiO, they are not orthogonal for FeO and CoO. Their overlap matrices $\chi_i^{(R)}$ and $\chi_i^{(A)}$ are given by

$$\begin{aligned}\chi^{(R)}_{i\ \nu_1\nu_2\nu_3,\nu_1'\nu_2'\nu_3'}&\equiv\langle R;i,\nu_1,\nu_2,\nu_3|R;i,\nu_1',\nu_2',\nu_3'\rangle\\&=n_{i\nu_1,i\nu_1'}n_{i\nu_2,i\nu_2'}\overline{n}_{i\nu_3,i\nu_3'}\\&\quad-n_{i\nu_1,i\nu_2'}n_{i\nu_2,i\nu_1'}\overline{n}_{i\nu_3,i\nu_3'},\end{aligned} \tag{2.10}$$

$$\begin{aligned}\chi^{(A)}_{i\ \nu_1\nu_2\nu_3,\nu_1'\nu_2'\nu_3'}&\equiv\langle A;i,\nu_1,\nu_2,\nu_3|A;i,\nu_1',\nu_2',\nu_3'\rangle\\&=\overline{n}_{i\nu_1,i\nu_1'}\overline{n}_{i\nu_2,i\nu_2'}n_{i\nu_3,i\nu_3'}\\&\quad-\overline{n}_{i\nu_1,i\nu_2'}\overline{n}_{i\nu_2,i\nu_1'}n_{i\nu_3,i\nu_3'}.\end{aligned} \tag{2.11}$$

In the presence of the nonorthogonality, the Hamiltonian matrices expanded within the three-particle states are to be modified from Eq. (2.16) in Ref. 49. With the notations $\Delta H\equiv H-\langle g|H|g\rangle$ and $\Delta N_e\equiv N_e-\langle g|N_e|g\rangle$, the Hamiltonian matrix for the retarded part is expressed as

$$\begin{aligned}[\hat{H}^{(R)}]_{i\nu_1\nu_2\nu_3;i\nu_1'\nu_2'\nu_3'}&\equiv\langle R;i,\nu_1,\nu_2,\nu_3|\Delta H-\mu_0\Delta N_e|R;i,\nu_1',\nu_2',\nu_3'\rangle\\&=n_{i\nu_1,i\nu_1'}n_{i\nu_2,i\nu_2'}\overline{\epsilon}_{i\nu_3,i\nu_3'}-n_{i\nu_1,i\nu_2'}n_{i\nu_2,i\nu_1'}\overline{\epsilon}_{i\nu_3,i\nu_3'}+n_{i\nu_1,i\nu_1'}\epsilon_{i\nu_2,i\nu_2'}\overline{n}_{i\nu_3,i\nu_3'}-n_{i\nu_1,i\nu_2'}\epsilon_{i\nu_2,i\nu_1'}\overline{n}_{i\nu_3,i\nu_3'}\\&\quad+\epsilon_{i\nu_1,i\nu_1'}n_{i\nu_2,i\nu_2'}\overline{n}_{i\nu_3,i\nu_3'}-\epsilon_{i\nu_1,i\nu_2'}n_{i\nu_2,i\nu_1'}\overline{n}_{i\nu_3,i\nu_3'}+n_{i\nu_1,i\nu_1'}g^{(1)}(i\nu_2,i\nu_3,i\nu_2',i\nu_3')\\&\quad+n_{i\nu_2,i\nu_2'}g^{(1)}(i\nu_1,i\nu_3,i\nu_1',i\nu_3')-n_{i\nu_1,i\nu_2'}g^{(1)}(i\nu_2,i\nu_3,i\nu_1',i\nu_3')-n_{i\nu_2,i\nu_1'}g^{(1)}(i\nu_1,i\nu_3,i\nu_2',i\nu_3')\\&\quad+\overline{n}_{i\nu_3,i\nu_3'}g^{(2)}(i\nu_1,i\nu_2,i\nu_1',i\nu_2'),\end{aligned} \tag{2.12}$$

with

$$\begin{aligned}g^{(1)}(i\nu_2,i\nu_3,i\nu_2',i\nu_3')&\equiv\sum_{\mu_1\mu_2\mu_3\mu_4}\tfrac{1}{2}g(\mu_1\mu_2\mu_3\mu_4)[-(n_{i\nu_2,i\mu_1}\overline{n}_{i\mu_2,i\nu_3'}\overline{n}_{i\nu_3,i\mu_4}n_{i\mu_3,i\nu_2'})\\&\quad-(\mu_1\leftrightarrow\mu_2,\mu_3\leftrightarrow\mu_4)+(\mu_1\leftrightarrow\mu_2)+(\mu_3\leftrightarrow\mu_4)],\end{aligned} \tag{2.13}$$

$$g^{(2)}(i\nu_1,i\nu_2,i\nu_1',i\nu_2') \equiv \sum_{\mu_1\mu_2\mu_3\mu_4} \tfrac{1}{2} g(\mu_1\mu_2\mu_3\mu_4) \times [(n_{i\nu_1,i\mu_1}n_{i\nu_2,i\mu_2}n_{i\mu_4,i\nu_2'}n_{i\mu_3,i\nu_1'}) + (\mu_1 \leftrightarrow \mu_2, \mu_3 \leftrightarrow \mu_4) - (\mu_1 \leftrightarrow \mu_2) - (\mu_3 \leftrightarrow \mu_4)]. \quad (2.14)$$

In Eq. (2.12), the second, third and fourth lines come from the HF on-site excitation energy for two electrons and one hole. The remaining terms represent interaction contributions. In Eqs. (2.13) and (2.14), the second, third and fourth terms in the square brackets are given by the first term, exchanging the indices as indicated in the round brackets. The Hamiltonian matrix $[\hat{H}^{(A)}]_{i\nu_1\nu_2\nu_3;i\nu_1'\nu_2'\nu_3'}$ for the advanced part is obtained by exchanging the role of the electron and hole in the expression for the retarded part. We do not set down this expression explicitly.

Treating carefully the nonorthogonality between the three-particle states, and using Eq. (2.12) and the corresponding form for the advanced part for the Hamiltonian matrix, we calculate the resolvent and thereby the self-energy. The Green's functions in the momentum representation $G^{dd}_{\tau m\sigma,\tau' m'\sigma'}(\mathbf{k},\omega), G^{pp}_{\tau l\sigma,\tau' l'\sigma'}(\mathbf{k},\omega)$ are calculated by inserting the self-energy into the Dyson equation. Here the indices τ and τ' designate the atoms in the unit cell. The Green's functions contain the chemical potential μ, which differs from its HF value μ_0. However, the shift of the chemical potential does not affect the shape of the spectral function where a large band gap is present. Therefore we do not determine the shift of the chemical potential, but simply assume that the Fermi level is located somewhere in the gap. Note that the Green's functions consist only of discrete poles on the real ω axis.

The spectral densities $\rho^d_\sigma(\omega)$ projected onto TM $3d$ orbits and $\rho^p_\sigma(\omega)$ projected onto O $2p$ orbits are evaluated from

$$\rho^d_\sigma(\omega) = -\mathrm{sgn}(\omega)\frac{1}{N\pi}\sum_{\mathbf{k}m} \mathrm{Im}G^{dd}_{\tau m\sigma,\tau m\sigma}(\mathbf{k},\omega),$$
$$\rho^p_\sigma(\omega) = -\mathrm{sgn}(\omega)\frac{1}{N\pi}\sum_{\mathbf{k}m} \mathrm{Im}G^{pp}_{\tau m\sigma,\tau m\sigma}(\mathbf{k},\omega), \quad (2.15)$$

where N represents the number of unit cell. Also the local spin moment M_d on TM sites is evaluated from

$$M_d = \mu_B \int_{-\infty}^{\mu} (\rho^d_\downarrow(\omega) - \rho^d_\uparrow(\omega)) d\omega. \quad (2.16)$$

III. RESULTS AND DISCUSSIONS

In this section we present results of calculations based on the tight-binding model with the parameter values given in Table I. We carry out the HF calculation self-consistently, thereby assuming an antiferromagnetic order of the second kind. We use a rhombohedral unit cell containing two TM atoms and two O atoms on a fcc lattice. By using 512 sample points in the first Brillouin zone, we continue the iteration until the sum of the square root of the HF self-energy converges with an error less than 10^{-7} eV. Then we make the self-energy correction to the HF solution by following the procedure given in Sec. II. For the sake of comparison, we also carry out an LDA calculation with the use of the muffin-tin Korringa-Kohn-Rostoker method. The results are essentially the same as those obtained by Terakura *et al.*[2]

TABLE II. Local-spin moment calculated by means of the LDA, the HF approximation, and including the self-energy correction in units of μ_B, in comparison with the experiments.

	LDA	HF	HF+Σ	Expt.
MnO	4.19	4.82	4.80	4.79 (Ref. 5), 4.58 (Ref. 8)
FeO	3.39	3.78	3.75	3.32 (Ref. 3)
CoO	2.31	2.77	2.74	3.35 (Ref. 6), 3.8 (Refs. 3 and 7)
NiO	0.94	1.75	1.72	1.77 (Ref. 5), 1.64 (Ref. 4), 1.90 (Ref. 8)

A. MnO

Table II lists the local spin moment calculated from Eq. (2.16) in comparison with experiments. The LDA underestimates the size of the local-spin moment. The HF approximation yields a larger value, leading a good agreement with the experiment. The calculated value $4.8\mu_B$ indicates that almost all five Mn $3d$ orbits are occupied by electrons with majority spin, due to Hund's rule coupling.

Figure 1 shows the spectral density of MnO. It is noticed that the LDA gives too small a band gap. The HF approximation increases the size of the band gap to 5 eV, in agreement with experiment. As for the valence band, both the LDA and the HF approximation give similar results. The

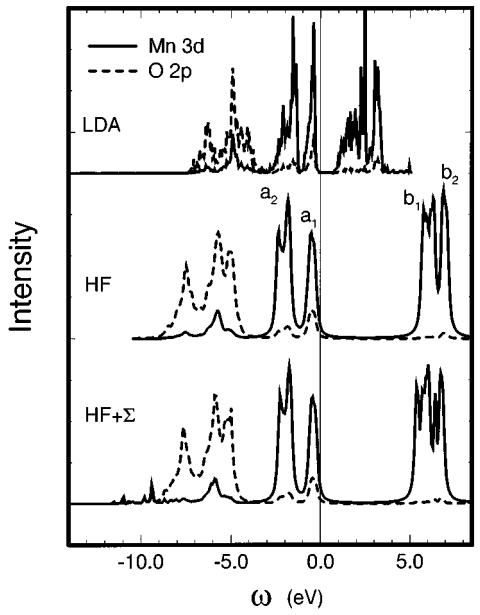

FIG. 1. Spectral densities projected onto Mn $3d$ states (solid lines) and O $2p$ states (broken lines), calculated by means of the LDA, the HF approximation, and including the self-energy correction. An imaginary part 0.01 eV is added to the HF energy eigenvalues. An imaginary part 0.01 eV is also added to the energy eigenvalues of $H^{(r)}$ and $H^{(a)}$. The origin of the ω axis is set at the top of the valence band.

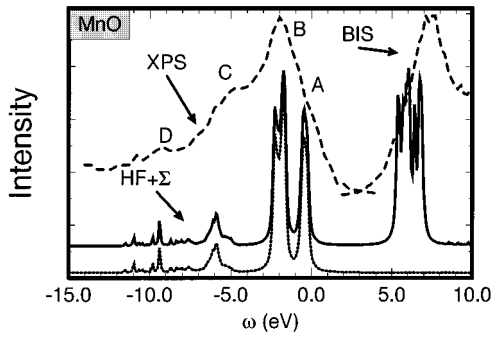

FIG. 2. Spectral density projected onto Mn $3d$ states (solid lines) in comparison with the XPS and BIS spectra (broken lines) for MnO. The dotted line shows the contribution of the majority-spin states.

spectral density projected onto Mn $3d$ states is mainly situated in the upper part of the valence band. Peaks a_1 and a_2 come from e_g and t_{2g} states with majority spin, respectively. On the other hand, the spectral density projected onto O $2p$ states is concentrated in the lower part of the valence band. At the top of the valence band it is smaller than the LDA value, suggesting an insulator of typical Mott-Hubbard type. The small O $2p$ character at the top of the valence band is due to the large value of Δ, which reduces the actual mixing between O $2p$ and Mn e_g orbits (σ bonding). The conduction band given by the HF approximation is quite different from the one given by the LDA. Peaks b_1 and b_2 come from t_{2g} and e_g states of Mn with minority spin, respectively.

The self-energy correction is found to be very small. It merely induces a weak satellite structure at $\omega \simeq -9$ eV below the valence band, and slightly reduces the size of the band gap from its HF value. One reason for the small self-energy is that electron-hole pair creations are much reduced when minority-spin states are nearly empty, as is the case for Mn.

Figure 2 shows the spectral density projected onto Mn $3d$ states in comparison with the XPS (Ref. 20) and BIS spectra.[21] The cross section in XPS experiments with $\hbar\omega > 10^3$ eV is an order of magnitude larger for the $3d$ orbits of Mn than for the $2p$ orbits of O. The XPS spectra consist of a shoulder A, a peak B, a broad structure C, and a satellite structure D. These structures are well reproduced in the HF calculation (no satellites exist in this approximation) and in the present theory. The experimental intensity around peak C looks larger than the calculated one, indicating that the contribution from the spectral density projected onto O $2p$ states should be added to the calculated XPS intensity in this energy region (the cross section for O $2p$ orbits is as much as about 18% of that for Mn $3d$ orbits).[21] Structure D corresponds to the excitation of three particles. The BIS spectra correspond roughly to the calculated spectra of the conduction band. They should not be directly compared to the calculated one, though, since Mn $4s$ states contribute substantially to the BIS spectra.

Figure 3 shows the dispersion relation of quasiparticles with momenta along the $\Gamma(0,0,0)$-$X(\pi/a,0,0)$ line (a denotes the lattice constant). Since the self-energy correction does not cause any appreciable change, we have omitted the results. For the valence band, the dispersion curves of the LDA are quite similar to those of the HF approximation. While the

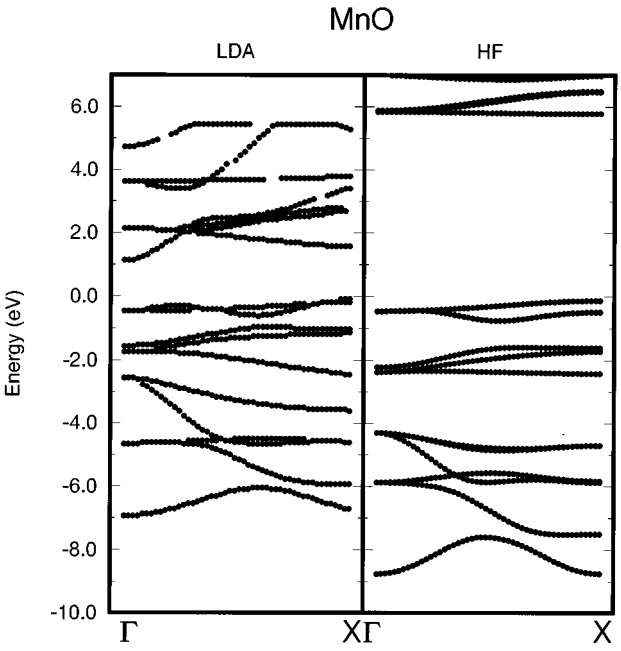

FIG. 3. Dispersion relation of quasiparticles with momenta along the $\Gamma(0,0,0)$-$X(\pi/a,0,0)$ line for MnO, calculated by means of the LDA, the HF approximation, and including the self-energy correction. The origin of quasiparticle energies is set at the top of the valence band.

curves near the upper part of the valence band are rather flat, they are very disperse at the lower part of the valence band. The former result mainly from Mn $3d$ states, while the latter result from O $2p$ states.

B. FeO

As shown in Table II, the HF approximation yields a value of $\sim 3.8\mu_B$ for the local-spin moment, which is larger than its LDA value. This suggests that each Fe atom is close to the high-spin state of the $3d^6$ configuration, a result of Hund's-rule coupling. Inclusion of the spin-orbit coupling may further increase the total magnetic moment by inducing an orbital moment. The experimental value of the local-spin moment is smaller than the calculated one. The reason for the discrepancy is unclear at present.

Figure 4 shows the spectral density of FeO. Although this material is an insulator, the LDA predicts a metallic ground state. The HF approximation leads to a band gap as large as 4 eV. Also it considerably changes not only the conduction-band but also the valence-band contributions. The spectral density consists of several peaks. Peak a_1 comes from the t_{2g} minority-spin states of Fe. They hardly mix with O $2p$ orbits (π bonding). On the other hand, peak a_2 comes from the e_g majority-spin states of Fe, which mix strongly with O $2p$ orbits. Therefore this peak contains a considerable number of O $2p$ states. Peak a_3 comes from the t_{2g} majority-spin states of Fe. On the lower part of the valence band ($\omega < -4$ eV), both Fe $3d$ and O $2p$ spectral densities are distributed with nearly equal strength over a wide range. The conduction band consists mainly of Fe $3d$ states. Peaks b_1 and b_2 come from the t_{2g} and e_g minority-spin states, respectively.

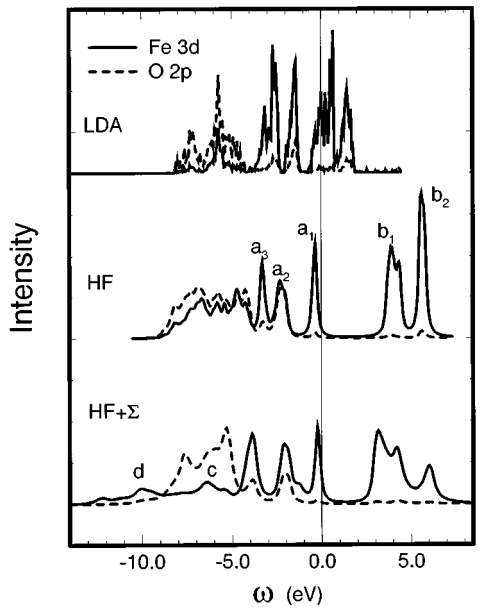

FIG. 4. Spectral density projected onto Fe $3d$ states (solid lines) and O $2p$ states (broken lines), calculated by means of the LDA, the HF approximation, and including the self-energy correction. An imaginary part 0.01 eV is added to the HF energy eigenvalues. An imaginary part 0.1 eV is also added to the energy eigenvalues of $H^{(r)}$ and $H^{(a)}$. The origin of the ω axis is set at the top of the valence band.

The self-energy correction is larger than that for MnO, and considerably modifies the spectral densities. The band gap is reduced to $\sim$3 eV from its HF value. A small satellite peak d is induced, and the Fe $3d$ spectral weight is strongly reduced in the lower part of the valence band (peak c). On the other hand, the peak positions a_1, a_2, and a_3 are nearly the same as in the HF approximation. This is a consequence of the presence of a pole at $\omega=-1$ eV in the self-energy, the contribution of which cancels the other ones in the upper part of the valence band. The spectral density projected onto O $2p$ states shows a reduction of peak a_2, and an increase in the lower part of the valence band. Note that near the top of the valence band the O $2p$ contribution is very small, indicating that the system is close to an insulator of the Mott-Hubbard type. As for the conduction band, a satellite is obtained near $\omega\simeq 6$ eV, and peaks b_1 and b_2 of the HF approximation are pushed down to lower excitation energies.

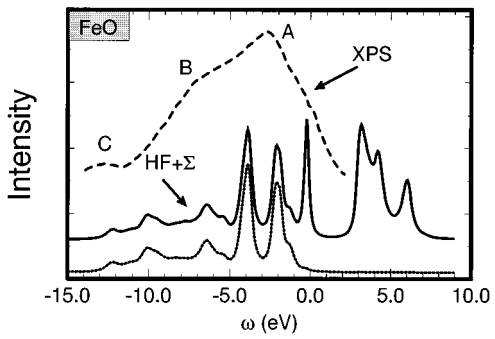

FIG. 5. Spectral density projected onto Fe $3d$ states (solid lines) in comparison with the XPS spectra (broken lines) for FeO. The dotted line shows the contribution of the majority spin states.

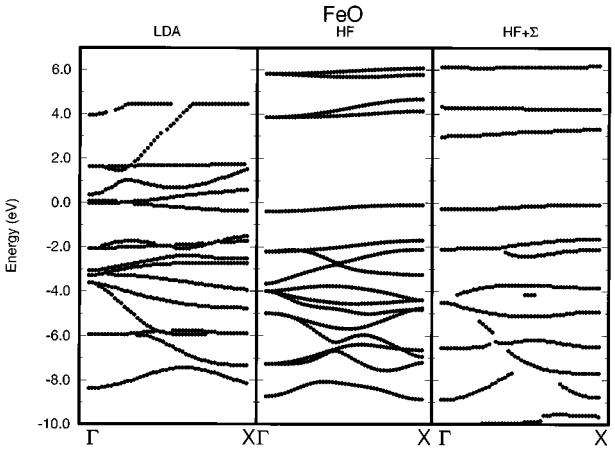

FIG. 6. Dispersion relation quasiparticles with momenta along the Γ-X line for FeO, by means of the LDA, the HF approximation, and including the self-energy correction. In the right panel, many flatbands coming from the poles of the self-energy are omitted when their intensities are weak. The origin of quasiparticle energies is set at the top of the valence band.

Figure 5 shows the spectral density projected onto Fe $3d$ states in comparison with the XPS spectra.[17] The XPS spectra consist of a broad peak A, a shoulder B, and a satellite C. The calculated spectra are in fair agreement with experiments; peak A corresponds well to peaks a_1, a_2, and a_3, and peaks B and C correspond well to peaks c and d. There exist no reliable BIS data for FeO.

Figure 6 shows the dispersion relation of quasiparticles with momenta along the Γ-X line. The dispersion curves of the HF approximation differ from those of the LDA.

C. CoO

Within the HF approximation the ground state of CoO is doubly degenerate. In the real system a crystal distortion of the Jahn-Teller type or an orbital ordering will lift this degeneracy. We expect, however, that such a change of the ground state does not cause any noticeable change in the excitation spectra, since the spectral densities are nearly independent for the two possible ground states. In the following, for the ground state we choose the one having cubic symmetry, where three t_{2g} states of Co are equally occupied by electrons.

The HF approximation gives a local-spin moment as large as $\sim 2.7\mu_B$. The self-energy correction changes this value very little. This suggests that each Co atom is close to the high-spin state of the $3d^7$ configuration. The calculated value is still smaller than the experimental one. We expect that inclusion of spin-orbit coupling increases it to a value closer to the experimental one, since the coupling is known to be large in CoO.

Figure 7 shows the spectral density of CoO. While the LDA predicts a metallic ground state, the HF approximation gives an insulating ground state with a large band gap of $\sim$4 eV. Several peaks are found in the upper part of the valence band; peak a_1 results from the t_{2g} minority-spin states of Co, while peak a_2 results from e_g majority-spin states of Co. In the middle and lower parts of the valence band, both Co $3d$

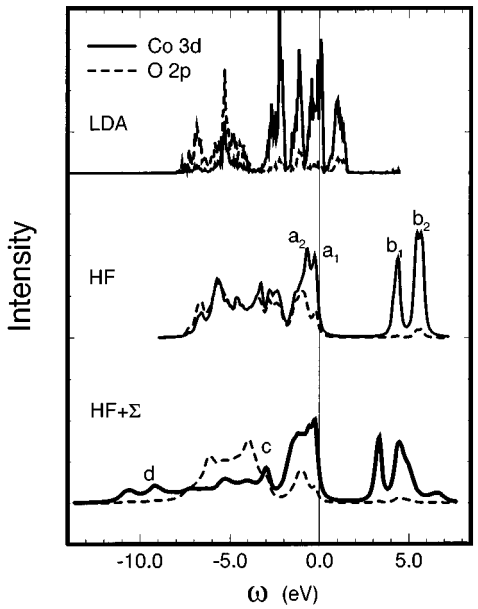

FIG. 7. Spectral densities projected onto Co $3d$ states (solid lines) and O $2p$ states (broken lines), calculated by means of the LDA, the HF approximation, and including the self-energy correction. Imaginary parts are added in the same way as for FeO. The origin of the ω axis is set at the top of the valence band.

and O $2p$ states are well mixed up, constituting a broad peak. The conduction band consists mainly of Co $3d$ states; peaks b_1 and b_2 result from the t_{2g} and e_g minority-spin states, respectively.

The self-energy correction strongly modifies the spectral densities. The band gap is reduced to $\sim$3 eV from its HF value. A satellite peak d is induced below the valence band, and another peak c emerges with strong three-particle character. The latter originates from a pole at $\omega \simeq -3$ eV in the self-energy. The spectral density projected onto Co $3d$ states is reduced in the lower part of the valence band, due to a transfer of spectral weight to the satellite and the upper part of the valence band. The O $2p$ states dominate the intensity in the lower part of the valence band, but their contribution is reduced at the top of the valence band. Thereby the system approaches an insulator of the Mott-Hubbard type. As regards the conduction band, the peaks b_1 and b_2 are shifted to lower excitation energies, and a satellite appears at $\omega \simeq 6.5$ eV.

Figure 8 shows the spectral density projected onto Co $3d$ states in comparison with the XPS and BIS spectra.[22] The XPS spectra consist of a peak A, a shoulder B, a broad structure C, and a satellite structure D. They correspond well to the peaks found in the present calculation. Around peak C, however, the XPS intensity looks larger than the calculated spectral density, as was the case for FeO. The difference may come from the contribution of O $2p$ states (the cross section of O $2p$ orbits is about 6% that of Co $3d$ orbits).[22] The BIS spectra correspond roughly to the calculated spectra for the conduction bands.

Figure 9 shows the dispersion relation of quasiparticles with momenta along the Γ-X line in comparison with the ARPS data.[11] In the ARPS data, a very flat dispersion is found around the top of the valence band, while in the

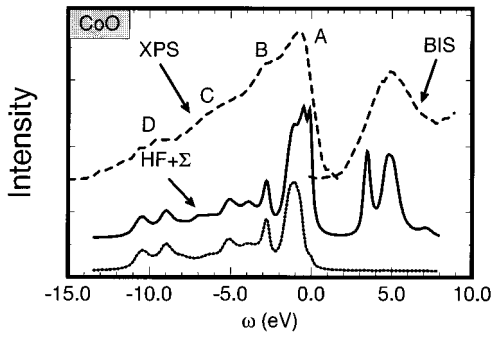

FIG. 8. Spectral density projected onto Co $3d$ states (solid lines) in comparison with the XPS and BIS spectra (broken lines) for CoO. The dotted line shows the contribution of the majority-spin states.

middle and lower parts of the valence band the curves are dispersive. In spite of the above-mentioned failures, the dispersion curves of the LDA fit the ARPS data rather well, as pointed out by Shen and co-workers.[10,11] This agreement is spoiled in the HF approximation. The self-energy correction again improves the agreement with experiments. The flatbands have strong Co $3d$ character, while the dispersive bands have strong O $2p$ character.

D. NiO

As shown in Table II, the local spin moment is underestimated in the LDA. The HF approximation improves the value, leading to good agreement with experiments. The self-energy correction changes this value little.

The spectral density has already been discussed in Ref. 49. We summarize that results and add a few details in the following. Within the LDA, the band gap is found to be very small. The spectral density projected onto Ni $3d$ states is concentrated in the upper part of the valence band, while that projected onto O $2p$ states is concentrated in the lower part

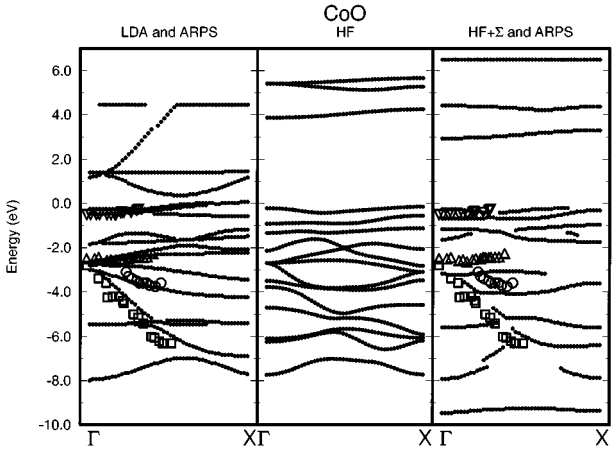

FIG. 9. Dispersion relation of quasiparticles with momenta along the Γ-X line for CoO, calculated by means of the LDA, the HF approximation, and including the self-energy correction. ARPS data are shown by symbols ∇, $\triangle$, $\bigcirc$, and $\square$. In the right panel, many flatbands coming from the poles of the self-energy are omitted when their intensities are weak. The origin of quasiparticle energies is set at the top of the valence band.

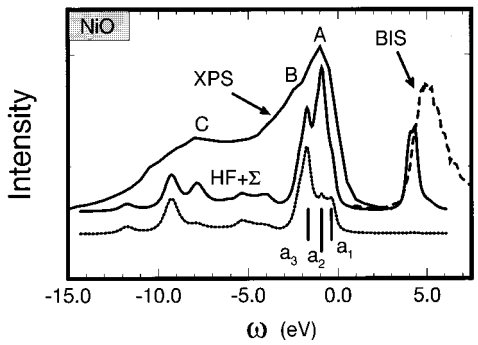

FIG. 10. Spectral densities projected onto Ni $3d$ states in comparison with the XPS and BIS spectra for NiO. The dotted line shows the contribution of the majority-spin states.

of the valence band. On the other hand, the HF approximation leads to a band gap of ~4 eV. At the top of the valence band, the weight of O $2p$ states is larger than that of Ni $3d$ states, implying an insulator of the charge-transfer type. The self-energy correction changes the spectrum obtained in the HF approximation drastically. It yields a satellite at $\omega \simeq -9$ eV. The spectral density projected onto Ni $3d$ states is reduced in the lower part of the valence band because the spectral density is transferred to the satellite and to the upper part of the valence band. The spectral density projected onto O $2p$ states is reduced in the upper part of the valence band, and enhanced in the lower part of the valence band. The weight of O $2p$ states is somewhat reduced at the top of the valence band, but still comparable to that of Ni $3d$ states. The system is close to an insulator of the charge-transfer type. See Fig. 4(a) in Ref. 49 for the spectral densities by means of the LDA, the HF approximation, and including the self-energy correction.

Figure 10 shows the spectral density projected onto Ni $3d$ states in comparison with the XPS (Ref. 23) and BIS spectra.[18] Shoulder a_1 at the top of the valence band comes mainly from the e_g majority-spin states, which mix considerably with O $2p$ orbits (σ bonding). Peaks a_2 and a_3 come mainly from the t_{2g} minority and majority-spin states, respectively. In the conduction band, a satellite structure is generated at $\omega \sim 5$ eV, and a peak is shifted to lower energies. These structures are in good agreement with the experiments. Note that the calculated spectral density projected onto O $2p$ states agrees also quite well with O $K\alpha$ XES,[50,53] as shown in Fig. 4(b) in Ref. 49.

Finally we mention the dispersion relation of quasiparticles in comparison with the ARPS data.[12] As in the case of CoO, the calculated curves show a number of nearly dispersionless bands and rather dispersive ones along the Γ-X line. The agreement between the experimental data and the calculated curves obtained in the LDA is partly reproduced by the self-energy correction, as shown in Fig. 3 in Ref. 49.

IV. CONCLUDING REMARKS

We developed a many-body theory by taking account of three-body correlations within a multiorbital tight-binding model for MnO, FeO, CoO, and NiO. In order to deal with the complexity of the multiorbital model, we used a local approximation for the three-particle scattering processes which are assumed to take place only on the transition-metal sites. The theory does not only contain ladder-type diagrams but also bubble-type ones. It is obviously insufficient to terminate a perturbation expansion in U after second order, because of large values of U.[54] We showed that the self-energy correction due to three-particle correlations greatly improves the excitation spectra obtained in the LDA and the HF approximation. It describes the itinerant character of quasiparticles as well as the localized one, and induces satellite structure with sufficient intensities. The results agree quite well with the experimental data of XPS, BIS, O $K\alpha$ XES, and ARPS.

In spite of the successes mentioned above, the present theory also has some drawbacks. One is that three-particle states are restricted within transition-metal sites. This neglects the corresponding correlations on O sites. It may also become inappropriate with decreasing values of the charge-transfer energy, since holes created in the intermediate states can move easily to neighboring O sites. Including such processes may enhance the spectral density projected onto O $2p$ states at the top of the valence band. Another drawback is that the present theory is unable to describe the lifetime broadening of spectral peaks. This is due to the restriction of the number of three-particle states in the local approximation. The original three-body scattering theory is able to describe such spectral widths.[41]

Recently Manghi, Calandra, and Ossicini[55] proposed a three-body scattering theory applying a ''local approximation'' directly to Faddeev's equation. Considering local three-body correlations, they obtained an excitation spectra for NiO which is similar to the present ones. An important difference is that in their calculation the self-energy correction is implemented on the quasiparticle energies of the LDA, not on those of the HF approximation. This may cause ambiguities, since the LDA already contains some parts of electron correlations. The three-body correlations result in an increase of the band gap in their theory, while in the present theory the gap is *reduced* from its HF value.

The present theory is related to a projection approach, which uses local operators for the description of electron correlations.[56] Both approaches give similar results for ferromagnetic Ni.[48,57] A quite different approach, which aims at the low-energy sector, is based on a strong-coupling theory of a generalized spin-fermion model.[58] It describes ARPS data for Ni semiquantitatively.

ACKNOWLEDGMENTS

We would like to thank P. Fulde for valuable discussions and a critical reading of the manuscript. Thanks are also due to N. Hamada and K. Terakura for helpful discussions. This work was supported in part by a Grant-in-Aid for Scientific Research from the Ministry of Education, Science, Sports and Culture, Japan.

[1] N. F. Mott, Proc. Phys. Soc. London, Sec. A **62**, 416 (1949); *The Metal Insulator Transition*, 2nd ed. (Taylor & Francis, London, 1974).
[2] K. Terakura, T. Oguchi, A. R. Williams, and J. Kübler, Phys. Rev. B **30**, 4734 (1984).
[3] W. L. Roth, Phys. Rev. **110**, 1333 (1958).
[4] H. A. Alperin, J. Phys. Soc. Jpn. Suppl. B **17**, 12 (1962).
[5] B. E. F. Fender, A. J. Jacobson, and F. A. Wegwood, J. Chem. Phys. **48**, 990 (1968).
[6] D. C. Khan and R. A. Erickson, Phys. Rev. B **1**, 2243 (1970).
[7] D. Herrmann-Ronzaud, P. Burlet, and J. Rossat-Mignod, J. Phys. C **11**, 2123 (1978).
[8] A. K. Cheetham and D. A. Hope, Phys. Rev. B **27**, 6964 (1983).
[9] G. K. Wertheim and S. Hüfner, Phys. Rev. Lett. **28**, 1028 (1972).
[10] Z.-X. Shen, C. K. Shih, O. Jepsen, W. E. Spicer, I. Lindau, and J. W. Allen, Phys. Rev. Lett. **64**, 2442 (1990).
[11] Z.-X. Shen, J. W. Allen, P. A. P. Lindberg, D. S. Dessau, B. O. Wells, A. Borg, W. Ellis, J. S. Kang, S.-J. Oh, I. Lindau, and W. E. Spicer, Phys. Rev. B **42**, 1817 (1990).
[12] Z.-X. Shen, R. S. List, D. S. Dessau, B. O. Wells, O. Jepsen, A. J. Arko, R. Barttlet, C. K. Shih, J. C. Huang, and P. A. P. Lindberg, Phys. Rev. B **44**, 3604 (1991).
[13] A. Fujimori and F. Minami, Phys. Rev. B **30**, 957 (1984).
[14] G. van der Laan, J. Zaanen, G. A. Sawatzky, R. Karnatak, and J.-M. Esteva, Phys. Rev. B **33**, 4253 (1986).
[15] K. Okada and A. Kotani, J. Phys. Soc. Jpn. **61**, 4619 (1992).
[16] A. Tanaka and T. Jo, J. Phys. Soc. Jpn. **63**, 2788 (1994).
[17] P. S. Bagus, C. R. Brundle, T. J. Chuang, and K. Wandelt, Phys. Rev. Lett. **39**, 1229 (1977).
[18] G. A. Sawatzky and J. W. Allen, Phys. Rev. Lett. **53**, 2339 (1984).
[19] S. Hüfner, Solid State Commun. **53**, 707 (1985).
[20] A. Fujimori, N. Kimizuka, T. Akahane, T. Chiba, S. Kimura, F. Minami, K. Siratori, M. Taniguchi, S. Ogawa, and S. Suga, Phys. Rev B **42**, 7580 (1990).
[21] J. van Elp, R. H. Potze, H. Eskes, R. Berger, and G. A. Sawatzky, Phys. Rev. B **44**, 1530 (1991).
[22] J. van Elp, J. L. Wieland, H. Eskes, P. Kuiper, G. A. Sawatzky, F. M. F. de Groot, and T. S. Turner, Phys. Rev. B **44**, 6090 (1991).
[23] J. van Elp, H. Eskes, P. Kuiper, and G. A. Sawatzky, Phys. Rev. B **45**, 1612 (1992).
[24] P. S. Bagus, G. Pacchioni, and F. Parmigiani, Chem. Phys. Lett. **207**, 569 (1993).
[25] M. R. Thuler, R. L. Benbow, and Z. Hurych, Phys. Rev. B **27**, 2082 (1983).
[26] A. Fujimori, N. Kimizuka, M. Taniguchi, and S. Suga, Phys. Rev. B **36**, 6691 (1987).
[27] J. M. Mckay, M. H. Mohamed, and V. E. Henrich, Phys. Rev. B **35**, 4304 (1987).
[28] J. Zaanen, G. A. Sawatzky, and J. W. Allen, Phys. Rev. Lett. **55**, 418 (1985).
[29] J. Hubbard, Proc. R Soc. London Ser. A **276**, 238 (1963); **277**, 237 (1964); **281**, 401 (1964).
[30] P. Kuiper, G. Kruizinga, J. Ghijsen, G. A. Sawatzky, and H. Verweij, Phys. Rev. Lett. **62**, 221 (1989).
[31] R. J. Lad and V. E. Henrich, Phys. Rev. B **38**, 10 860 (1988).
[32] N. B. Brookes, D. S.-L. Law, D. R. Warburton, P. L. Wincott, and G. Thornton, J. Phys. Condens. Matter **1**, 4267 (1989).
[33] Z.-X. Shen and D. S. Dessau, Phys. Rep. **253**, 1 (1995).
[34] V. I. Anisimov, J. Zaanen, and O. K. Andersen, Phys. Rev. B **44**, 943 (1991).
[35] A. Svane and O. Gunnarsson, Phys. Rev. Lett. **65**, 1148 (1990).
[36] Z. Szotek, W. M. Temmerman, and H. Winter, Phys. Rev. B **47**, 4029 (1993).
[37] M. Arrai and T. Fujiwara, Phys. Rev. B **51**, 1477 (1995).
[38] L. Hedin, Phys. Rev. **139**, A796 (1965); L. Hedin and S. Lundqvist, in *Solid State Physics*, edited by H. Ehrenreich, F. Seitz, and D. Turnbull (Academic, New York, 1969), Vol. 23, p. 1.
[39] F. Aryasetiawan and O. Gunnarson, Phys. Rev. Lett. **74**, 3221 (1995).
[40] M. D. Towler, N. L. Allan, N. M. Harrison, V. R. Saunders, W. C. Mackrodt, and E. Aprá, Phys. Rev. B **50**, 5041 (1994).
[41] J. Igarashi, J. Phys. Soc. Jpn. **52**, 2827 (1983); **54**, 260 (1985).
[42] J. Igarashi, in *Core-Level Spectroscopy in Condensed Systems*, edited by J. Kanamori and A. Kotani (Springer, Berlin, 1988), p. 168.
[43] J. Kanamori, Prog. Theor. Phys. **30**, 275 (1963).
[44] A. Liebsch, Phys. Rev. Lett. **43**, 1431 (1979).
[45] A. Liebsch, Phys. Rev. B **23**, 5203 (1981).
[46] J. A. Hertz and D. M. Edwards, J. Phys. F **3**, 2174 (1973); **3**, 2191 (1973).
[47] L. D. Faddeev, Zh. Eksp. Teor. Fiz. **39**, 1459 (1960) [Sov. Phys. JETP **12**, 1014 (1961)].
[48] J. Igarashi, P. Unger, K. Hirai, and P. Fulde, Phys. Rev. B **49**, 16 181 (1994).
[49] M. Takahashi and J. Igarashi, Ann. Phys. **5**, 247 (1996).
[50] N. Wassdahl, P. Bleckert, G. Gray, P. Glans, N. Martensson, J. Nordgren, J.-E. Rubensson, R. Nyholm, and S. Cramm, in *X-Ray and Inner-Shell Processes*, edited by T. A. Carlson, M. O. Krauss, and S. T. Manson, AIP Conf. Proc. No. 215 (AIP, New York, 1990), pp. 451–464.
[51] J. C. Slater and G. F. Koster, Phys. Rev. **94**, 1498 (1954).
[52] L. F. Mattheiss, Phys. Rev. **5**, 290 (1972); **5**, 306 (1972).
[53] V. I. Anisimov, P. Kuiper, and J. Nordgren, Phys. Rev. B **50**, 8257 (1994).
[54] T. Mizokawa and Fujimori, Phys. Rev. B **53**, R4201 (1996).
[55] F. Manghi, C. Calandra, and S. Ossicini, Phys. Rev. Lett. **73**, 3129 (1994).
[56] P. Fulde, *Electron Correlation in Molecules and Solids* (Springer, Berlin, 1991).
[57] P. Unger, J. Igarashi, and P. Fulde, Phys. Rev. B **50**, 10 485 (1994).
[58] J. Bala, A. M. Oleś, and J. Zaanen, Phys. Rev. Lett. **72**, 2600 (1994).